Ca^{2+} Diffusion within the Presynaptic Terminal

Zihan Zhang (Steven)*

November 8, 2022

This project is supervised by Professor Charles S. Peskin, Courant Institute, and serves as the first course-project in his course *Special Topic: Modeling and Simulation in Science, Engineering, and Economics* in the Fall 2022 semester.

1 Introduction

In the late 1970s, a voltage clamp study of the presynaptic terminal in squid stellate ganglion has given quantitative results relating inward Ca^{2+} current to presynaptic membrane potential and postsynaptic response to inward Ca^{2+} current [1]. Later, quantitative modeling suggested that in presynaptic terminals, the intracellular calcium concentration profile during inward calcium current could be characterized by discrete peaks of calcium immediately adjacent to the calcium channels, as the medium of transmitter release [2]. Here we integrate these two models and simulate the Ca^{2+} diffusion within the presynaptic terminal, where the model's logic, formulation, and structure are largely based on Peskin's lecture note [3]. The transmitter-laden vesicles of the presynaptic terminal release their contents into the synaptic cleft at specialized membrane sites. Release involves the fusion of the vesicle membrane and the cell membrane, which requires the presence of Ca^{2+} within the presynaptic terminal. The vesicle release site is close to the Ca^{2+} concentration for vesicle release is the *local* concentration at some distance from the channel. The local concentration can be much higher than the general concentration of free Ca^{2+} within the presynaptic channel.

2 Assumptions

We make the following assumptions to simplify the model and preserve the characterization of salient physiological features [3]:

1. Each release site has its own Ca^{2+} channel.
2. The presynaptic terminal looks to each channel like a half-space with a plane boundary (the membrane) containing a source at one point in the boundary (the channel).
3. The Ca^{2+} concentration approaches zero with increasing distance from the channel.
4. The Ca^{2+} concentration profile near the channel rapidly achieves a steady state.
5. Assumes all Ca^{2+} channels share the same physiological feature.

3 Equations

3.1 Presynaptic Ca^{2+} channel

According to the constant-field model, the current through a single Ca^{2+} channel is [1]:

$$i_{\text{Ca}} = (2q)\frac{aD}{\ell}\left(\frac{2qv}{kT}\right)\frac{[\text{Ca}^{2+}]_{\text{in}}\exp\left(\frac{2qv}{kT}\right) - [\text{Ca}^{2+}]_{\text{out}}}{\exp\left(\frac{2qv}{kT}\right) - 1}. \tag{1}$$

Here q the elementary charge, a the cross-sectional area of channel, ℓ channel length, D the diffusion coefficient of Ca^{2+}, k the Boltzmann's constant, T the absolute temperature, $[Ca^{2+}]_{\text{in/out}}$ the Ca^{2+} concentration inside/outside

*zz2589@nyu.edu

cell, v the membrane potential (inside minus outside), and i_{Ca} the Ca^{2+} current which is considered positive if outward. The free Ca^{2+} in cells is very low for the Ca^{2+} is actively pumped out of the cell or into intracellular organelles or heavily buffered [3]. We could make the approximation that $[Ca^{2+}]_{\text{in}} \sim 10^{-7}M \approx 0$ and $[Ca^{2+}]_{\text{out}} \sim 10^{-3}M$ [4]. ℓ is equivalent to membrane thickness, approximately $10nm$ [5]. The radius of Ca^{2+} ions is $0.231nm$, so we estimate the radius of channel r is $0.5nm$ and hence calculate a. We also estimate $\frac{q}{kT} \approx 25mV$ since the variation of T is negligible in reaction. Also, the flux (always inward) is:

$$f_{\text{Ca}} = -\frac{i_{\text{Ca}}}{2q}. \tag{2}$$

The single-channel flux would shrink to 0 when the membrane potential is large. The process of Ca^{2+} channel is also formulated [1]: each channel has 5 independent subunits, and each subunit has 2 states (Figure 1) with $\alpha_s^0 = 2ms^{-1}$ and $\beta_s^0 = 1ms^{-1}$. The channel is open when all 5 subunits are in the state S^*.

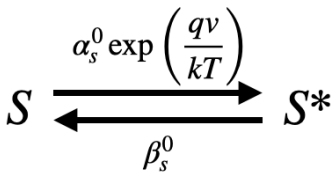

Figure 1: Transition paradigm between 2-states [3].

Let $\bar{N}_{\text{Ca}}$ be the total number of Ca^{2+} channels (assumed large) and let s be the fraction of subunits in the state S^*. The number of open channels is:

$$N_{\text{Ca}} = \bar{N}_{\text{Ca}} s^5, \tag{3}$$

and s satisfies:

$$\frac{ds}{dt} = \alpha_s^0 \exp\left(\frac{qv}{kT}\right)(1-s) - \beta_s^0 s. \tag{4}$$

We define $p_{\text{Ca}} = aD/\ell$ as the single-channel Ca^{2+} permeability. Thus, we could calculate the steady-state Ca^{2+} quantities:

$$\begin{aligned} s = s_\infty(v) &= \frac{2\exp\left(\frac{qv}{kT}\right)}{2\exp\left(\frac{qv}{kT}\right)+1}, \\ F_{\text{Ca}} = N_{\text{Ca}} f_{\text{Ca}} = (F_{\text{Ca}})_\infty(v) &= \bar{N}_{\text{Ca}} p_{\text{Ca}} [Ca^{2+}]_{\text{out}} \left(\frac{2\exp\left(\frac{qv}{kT}\right)}{2\exp\left(\frac{qv}{kT}\right)+1}\right)^5 \left(\frac{\left(\frac{2qv}{kT}\right)}{\exp\left(\frac{2qv}{kT}\right)-1}\right). \end{aligned} \tag{5}$$

Next, consider the response of the Ca^{2+} flux to a voltage step, which would be numerically implemented in later section [3]. Let the step go from $v_1 \to v_2$ and occur at $t = 0$. Prior to $t = 0$, the system has been in a constant state for a long time, so $s = s_\infty(v_1)$ and $F_{\text{Ca}} = (F_{\text{Ca}})_\infty(v_1)$. For $t > 0$, we have:

$$\tau_s(v_2)\frac{ds}{dt} = s_\infty(v_2) - s, \tag{6}$$

with $s(0) = s_\infty(v_1)$. That has the solution:

$$s(t) = s_\infty(v_2) + (s_\infty(v_1) - s_\infty(v_2))\exp\left(\frac{-t}{\tau_s(v_2)}\right). \tag{7}$$

Then for $t > 0$:

$$F_{\text{Ca}}(t) = \bar{N}_{\text{Ca}}[Ca^{2+}]_{\text{out}} \left\{ s_\infty(v_2) + (s_\infty(v_1) - s_\infty(v_2))\exp\left(\frac{-t}{\tau_s(v_2)}\right)\right\}^5 \cdot A\left(\frac{2qv_2}{kT}\right). \tag{8}$$

where:

$$A(\theta) = \frac{\theta}{\exp(\theta)-1}. \tag{9}$$

We remark that $F_{\text{Ca}}(t)$ is not continuous at $t = 0$. When the voltage jumps, the number of open Ca^{2+} channels does not change instantaneously, since $s(t)$ is continuous, but the flux of Ca^{2+} through each open channel suffers a jump. Thus:

$$\begin{aligned} F_{\text{Ca}}(0^-) &= (F_{\text{Ca}})_\infty(v_1), \\ F_{\text{Ca}}(0^+) &= (F_{\text{Ca}})_\infty(v_1)\frac{A(2qv_2/kT)}{A(2qv_1/kT)}. \end{aligned} \tag{10}$$

3.2 Ca^{2+} Diffusion

For an open channel, we use Equation (2) to model f_{Ca}; for a closed channel, $f_{\text{Ca}} = 0$. We use a spherically symmetric solution to the steady-state diffusion problem since such a solution is consisted with the boundary condition of no flux through the membrane except at the channel. Let $J_{\text{Ca}}(r)$ be the flux per unit area at radius r. According to Fick's law of diffusion:

$$J_{\text{Ca}} = -D\frac{\partial}{\partial r}[Ca^{2+}]. \tag{11}$$

In the steady state, the flux through an arbitrary hemisphere at radius r must equal the flux through the channel [3]:

$$\begin{aligned} f_{\text{Ca}} &= 2\pi r^2 J_{\text{Ca}} = -2\pi r^2 D\frac{\partial[Ca^{2+}]}{\partial r}, \\ [Ca^{2+}] &= \int_r^\infty \frac{f_{\text{Ca}}}{D2\pi(r')^2}dr' = \frac{f_{\text{Ca}}}{D2\pi r}. \end{aligned} \tag{12}$$

Thus, the Ca^{2+} concentration at a distance r_0 from the open channel is given by:

$$[Ca^{2+}]_{\text{site}} = [Ca^{2+}]_{\text{out}} \cdot \frac{a}{2\pi r_0 \ell}\frac{\left(\frac{2qv}{kT}\right)}{\exp\left(\frac{2qv}{kT}\right) - 1}. \tag{13}$$

Considering the average size of human cells, we define r as $10\mu m$ [6]. One model's key feature is the diffusion coefficient D drops out, and we get simple proportionality between the external Ca^{2+} concentration and the concentration at the side of the vesicle release when the channel is open. The proportionality involves the dimensionless geometric parameters ($\frac{a}{r_0\ell}$) and the dimensionless membrane potential parameter ($\frac{2qv}{kT}$). When the channel is closed, $[Ca^{2+}]_{\text{site}} = 0$ [3].

3.3 Release of vesicles from the presynaptic terminal

We know that the $[Ca^{2+}]$ concentration at the release site has a switch-like character. Thus, the membrane site at the Ca^{2+} channel forms a complex, and the kinetics of vesicle release can only be described by considering all possible states of that complex (Figure 2). When the channel is open, Ca^{2+} appears at the vesicle release site (M). The free vesicles are denoted as V, and MV represents a site with a vesicle bound, ready for release. When a release occurs, the vesicle is destroyed, the free membrane site M is regenerated and n molecules of the transmitter are dumped into the synaptic cleft.

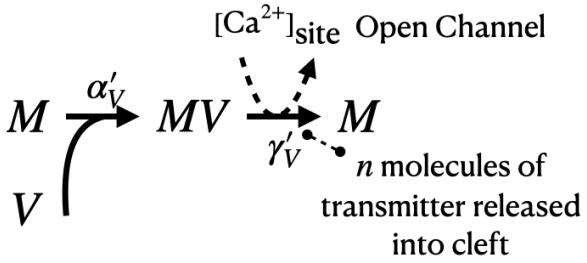

Figure 2: Complex of vesicle is bounded and destroyed [3].

Suppose:

$$\alpha_V = \alpha'_V[V] \tag{14}$$

by assuming the vesicle concentration $[V]$ in the presynaptic terminal is effectively constant. Thus, α is the first-order rate constant (probability per unit time) for the reaction $M \to MV$. Similarly, let:

$$\gamma_V = \gamma_V' [\text{Ca}^{2+}]_{\text{out}} \cdot \frac{a}{2\pi r_0 \ell} \frac{\left(\frac{2qv}{kT}\right)}{\left(\frac{2qv}{kT}\right) - 1} \tag{15}$$

Then γ_V is also the first-order rate constant for the reaction $MV \to M$ when the Ca^{2+} channel is open. When the Ca^{2+} channel is closed, the reaction $MV \to M$ cannot occur [3]. To define the states, we have:

$$\begin{aligned} X_k &= S_{5-k} S_k^* MV \\ Y_k &= S_{5-k} S_k^* M \end{aligned} \tag{16}$$

where $k \in [0, 5]$. Figure 3 describes the possible states and respective transitions in between. Notice that α_s and γ_V are voltage-dependent, whereas β_s and α_V are constants.

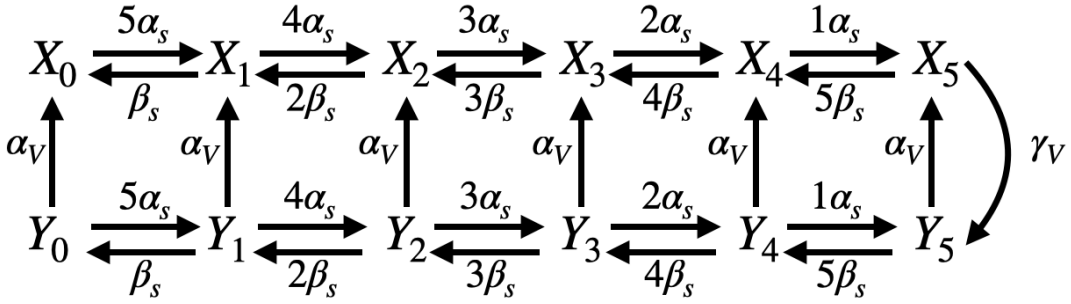

Figure 3: Complete state diagram for the channel - release site complex [3].

3.4 Hodgkin-Huxley Equations

As described in Peskin's note and applied in many experiments, people would use voltage-clamp (VClamp) to change membrane potential v and increase the intracellular voltage away from the resting potential ($\approx -80mV$). Such change would open the channels (with a certain probability rate) and the membrane site has a vesicle bound and ready for lease. Due to the high membrane potential (and the negligible Ca^{2+} current), the release does not occur instantaneously but until the voltage jumps back to a lower level. Here $v(t)$ is a rectangular function.

To simulate the cell's behavior and characterize $v(t)$ in a more physiologically reasonable way, we would implement Hodgkin-Huxley (HH) model, as the most fundamental biophysical mechanism and conductance-based model for the generation of an action potential [7]. More details could be seen in many papers and standard textbooks [8, 9, 10]. According to the HH model, an action potential is produced by an interplay of voltage-gated Na^+ and K^+ ion current (I_{Na} and I_{K}). $I_{\text{Na}}/I_{\text{K}}$ is an inward/outward current and tends to depolarize/hyperpolarize the neural membrane. We can write $I_{\text{Na}} = g_{\text{Na}}(V - E_{\text{Na}})$ and $I_{\text{K}} = g_{\text{K}}(V - E_{\text{K}})$, except that the conductances g_{Na} and g_{K} are not constant but gated by membrane potential V. Specifically, the potassium conductance $g_{\text{K}} = \bar{g}_{\text{K}} n^4$, where n is the activation gating variable. The idea is that n represents a fraction of gates in an open state, and $n-1$ is the fraction of gates in a closed state. The gating variable n obeys a dynamical equation according to first-order chemical kinetics:

$$\frac{dn}{dt} = \alpha_n(1 - n) - \beta_n n \tag{17}$$

with the opening and closing rates α_n and β_n dependent on V. This equation can be rewritten as $dn/dt = (n_\infty - n)/\tau_n$ with the steady-state $n_\infty = \alpha_n/(\alpha_n + \beta_n)$ and time constant $\tau_n = 1/(\alpha_n + \beta_n)$. The sodium conductance g_{Na} has not only an activation gating variable m but also an inactivation gating variable h such that $g_{\text{Na}} = \bar{g}_{\text{Na}} m^3 h$ with m and h described by similar first-order kinetic equations as for n but different opening and

closing rates. Thus, the HH model consists of four differential equations:

$$\begin{aligned} C_m \frac{dV}{dt} &= -g_L(V - E_L) - \bar{g}_{Na} m^3 h(V - E_{Na}) - \bar{g}_K n^4 (V - E_K) + I_{app}, \\ \frac{dm}{dt} &= \frac{(m_\infty(V) - m)}{\tau_m(V)} = \phi_m(\alpha_m(V)(1 - m) - \beta_m(V)m), \\ \frac{dh}{dt} &= \frac{(h_\infty(V) - h)}{\tau_h(V)} = \phi_h(\alpha_h(V)(1 - h) - \beta_h(V)h), \\ \frac{dn}{dt} &= \frac{(n_\infty(V) - n)}{\tau_n(V)} = \phi_n(\alpha_n(V)(1 - n) - \beta_n(V)n). \end{aligned} \tag{18}$$

where I is the injected current (in $\mu A/cm^2$). The parameters ϕ_{x} are the temperature factors, equal to 1 in the original HH model. The rate functions and other parameters, like conductances, reversal potentials, and passive time constant, are also explicitly defined [7]. In this simulation, we denote resting potential $V_0 = -70mV$ and the initial conditions of gating variables as $n_0 = 0.3, m_0 = 0.5, h_0 = 0.06$.

4 Numerical Methods

The numerical methods implemented in this project are standard, classical, and widely applied in many programming languages, well introduced in textbooks, and explained during lectures [11]. For completeness, we shortly address the essence here.

4.1 Dormand–Prince Method

To simulate the state diagram (Figure 3), we use the solver `ode45` to solve the nonstiff differential equations, which is based on an explicit Runge-Kutta (4,5) formula, the Dormand-Prince pair [12, 13]. It is a single-step solver: in computing $y(t_n)$, it needs only the solution at the immediately preceding time point $y(t_{n-1})$. Consider the initial value problem is specified:

$$\frac{dy}{dt} = f(t, y), \;\; y(t_0) = y_0. \tag{19}$$

Consider the explicit Runge-Kutta (RK) methods, we have:

$$y_{n+1} = y_n + h \sum_{i=1}^{s} b_i k_i, \tag{20}$$

where:

$$\begin{aligned} k_1 &= f(t_n, y_n), \\ k_2 &= f(t_n + c_2 h, y_n + h(a_{21} k_1)), \\ &\vdots \\ k_s &= f(t_n + c_s h, y_n + h(a_{s1} k_1 + a_{s2} k_2 + ... + a_{s,s-1} k_{s-1})) \end{aligned} \tag{21}$$

from which we could generate the Butcher tableau [11]. A Taylor series expansion shows that the RK method is consistent if and only if:

$$\sum_{i=1}^{s} b_i = 1, \;\; \sum_{j=1}^{i-1} a_{ij} = c_i, i = 2, ..., s. \tag{22}$$

Following this formulation, the Dormand-Prince Method would use 6 function evaluations to calculate fourth- and fifth-order accurate solutions. Its detailed coefficient setting is noted in the original literature [13]. We will use `ode45` to simulate the dynamics in Figure 3. Considering $\mathbf{X} = \{X_0, X_1, ..., Y_0, Y_1, ..., Y_5\}$, we set the initial condition as their steady states and define respective time derivatives. For instance:

$$\frac{dX_0}{dt} = \alpha_V Y_0 - 5\alpha_s X_0 + \beta_s X_1 \tag{23}$$

We generate a vector of $d\mathbf{X}$, input them into `ode45` solver in `Matlab`, and define the options, like relative and absolute error tolerance and maximum step size, then we would solve $\mathbf{X}$ numerically.

4.2 Explicit Forward Euler Method

To simulate Equation (18), we simply use Forward Euler (FE) method. Denote the time at the nth time-step by t_n and the computed solution at the nth time-step by y_n, $y_n \equiv y(t = t_n)$. The constant step size h is $h = t_n - t_{n-1}$. Given (t_n, y_n), the FE method computes y_{n+1} as:

$$y_{n+1} = y_n + hf(y_n, t_n) \tag{24}$$

5 Validation

5.1 Characterize membrane potential as rectangular function

We propose a simple experimental manipulation of the presynaptic membrane potential to test the validity of the code [3]:

1. Let the voltage stay at root $\frac{qv_1}{kT} = -3$ for a long time.
2. Step the voltage up for a level where $\frac{qv_2}{kT} \gg 1$ and hold it there for a while.
3. Step the voltage back down to rest, hold it there, and count the number of vesicles released. Each release event causes a EPSP or IPSP in the postsynaptic membrane potential.

By definition of the reaction rate by v, the system would sequentially switch to absorbing state $X_0 \to X_5 \to X_0$ [3]. Details depend on the parameter settings for γ_V', α_V and v_2, like the magnitude of pulse for X_5 and the peak for Y_5. Figure 4 describes the dynamic of the membrane potential and states when each step holds for $10ms$. At $t = 0$, $X_0 = 1$ and other states are 0. X_5 rapidly approaches the steady state in Step 2 and X_0 would change more gradually in Step 1 and 3. The simulation is consistent with the theory [3].

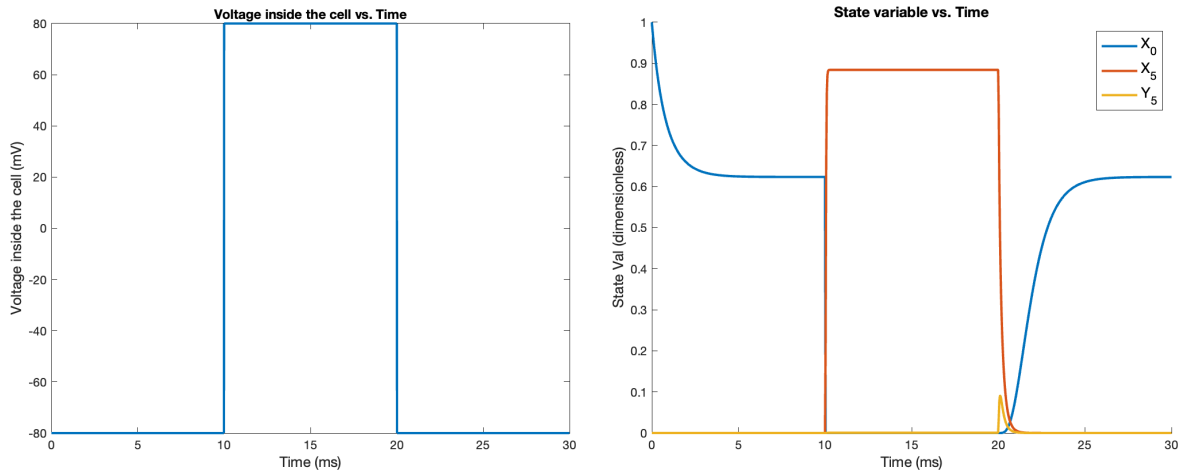

Figure 4: Change of membrane potential $v_1 \to v_2 \to v_1$ (left) and corresponding dynamics of cardinal states (right).

5.2 Repetitive firing through Hopf bifurcation in Hodgkin-Huxley model

We could check the validity of code by testing whether it satisfies repetitive firing, as a classical and well-studied property of the Hodgkin-Huxley model. Numerical simulations show that the HH model exhibits repetitive firing in response to steady I_{app} within a certain range of values [14, 15]. Generally, the firing rate increases and the amplitude of spikes decreases with increasing current. If I_{app} is too large V settles to a stable depolarized level, which is called depolarization block [9]. Figure 5 describes such a property, which strengthens the validity of our simulation.

6 Results and Discussion

Firstly, we formulate the membrane potential $v(t)$ as a rectangular function: it originally stays at the resting potential $-80mV$ and instantaneously increases to v_2. Upon different v_2, we calculate the fraction of open channels (steady-state), the single-channel Ca^{2+} current, and total $[Ca^{2+}]_{\text{site}}$. Figure 6 describes the results, which are

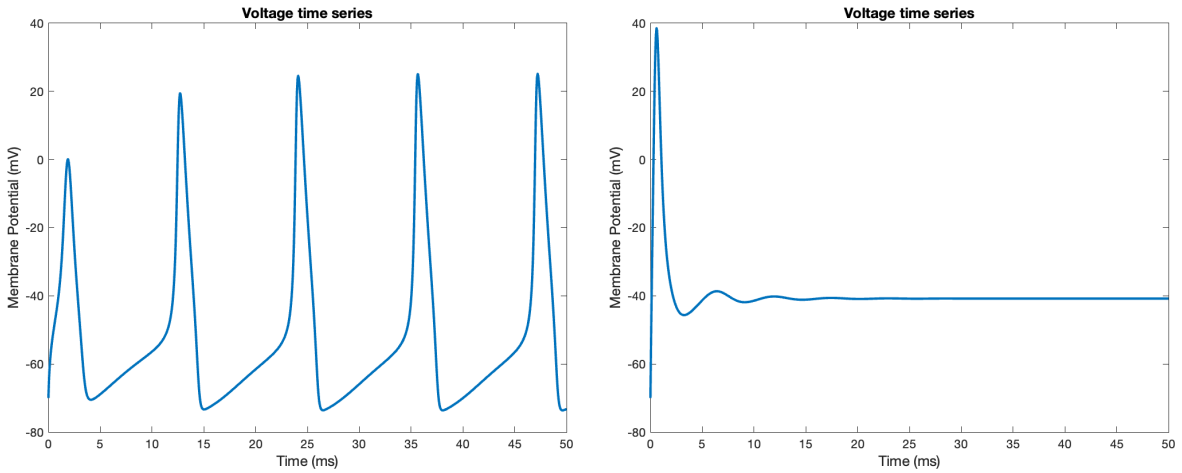

Figure 5: Action potential of Hodgkin-Huxley model when injection current $I_{\text{app}} = 20nA$ (left) and $= 200nA$ (right).

consistent with the theory [3]. Specifically, the Ca^{2+} current through the open channel is negligible when the membrane potential is high. Also, when the reaction rates are (partially) voltage-gated, the channel's opening rate is S-shaped. Plus, the total Ca^{2+} concentration at the site (multiplied with the opening rate) is parabolic and mostly symmetric, which approaches maximum when $v \approx 20mV$.

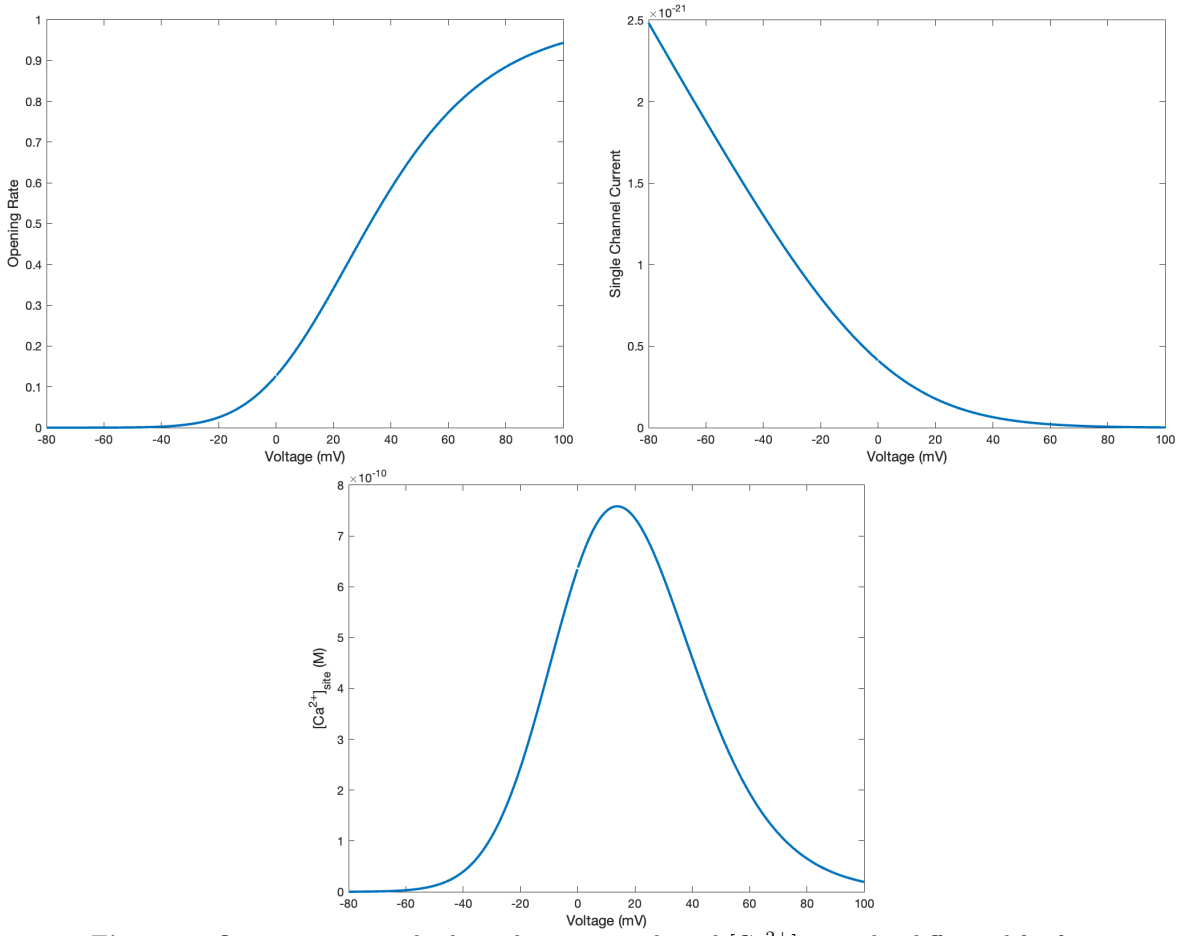

Figure 6: Opening rate, single-channel current, and total $[Ca^{2+}]_{\text{site}}$ under different lift of v.

We also use Hodgkin-Huxley model to simulate action potential towards the injection current and describe $v(t)$. Figure 7 simulates the dynamics of X_0, X_5, Y_5 under different injection current. As expected, the process is periodic and the magnitude for each pulse of X_5 (as the opening rate) is not very high, since the action potentials are small and not long-lasting (with approximately $5ms$ duration). The periodicity of pulses is identical with the action potential in HH model.

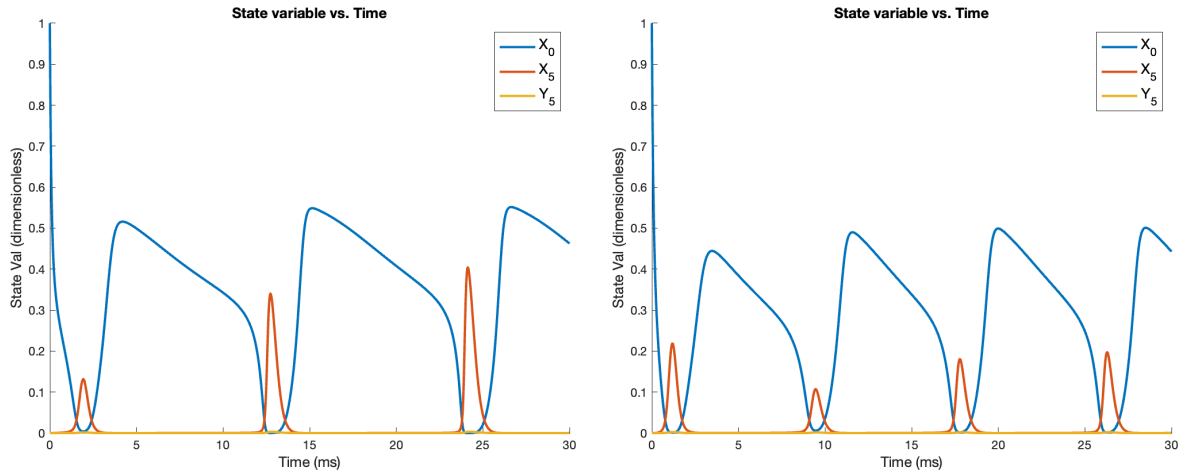

Figure 7: Dynamics of cardinal states when $v(t)$ is described by Hodgkin-Huxley model and $I_{\text{app}} = 20nA$ (left) and $= 50nA$ (right).

7 Conclusion

In this project, we model the presynaptic Ca^{2+} channel and diffusion (and vesicle release) within the presynaptic terminal during on-transient and off-transient. The membrane potential is formulated either by rectangular function or the Hodgkin-Huxley model. Our model captures and accomplishes many salient features of Ca^{2+} channel and diffusion as described in Peskin's lecture notes [3]. All the chosen hyperparameters are physiologically reasonable.

8 Source Code

All source code are written in `Matlab R2022b` and publicly available on the GitHub repository here.

References

[1] Rodolfo Llinás, Izchak Z. Steinberg, and Kerry Walton. "Presynaptic calcium currents and their relation to synaptic transmission: Voltage clamp study in squid giant synapse and theoretical model for the calcium gate". In: *Proceedings of the National Academy of Sciences* 73.8 (1976), pp. 2918–2922. DOI: 10.1073/pnas.73.8.2918. eprint: https://www.pnas.org/doi/pdf/10.1073/pnas.73.8.2918. URL: https://www.pnas.org/doi/abs/10.1073/pnas.73.8.2918.

[2] S.M. Simon and R.R. Llinás. "Compartmentalization of the submembrane calcium activity during calcium influx and its significance in transmitter release". In: *Biophysical Journal* 48.3 (1985), pp. 485–498. ISSN: 0006-3495. DOI: https://doi.org/10.1016/S0006-3495(85)83804-2. URL: https://www.sciencedirect.com/science/article/pii/S0006349585838042.

[3] Charles S. Peskin. "Lecture Note: Mathematical aspects of neurophysiology". In: (2000). URL: https://www.math.nyu.edu/~peskin/neuronotes/index.html.

[4] Timothy J. B. Simons. "Calcium and neuronal function". In: *Neurosurgical Review* 11 (2005), pp. 119–129.

[5] R. Hine. *The Facts on File Dictionary of Biology*. FOF Science Library. Facts On File, Incorporated, 2009. ISBN: 9781438109350. URL: https://books.google.com/books?id=bEuTESL21iUC.

[6] Miriam Ginzberg, Ran Kafri, and Marc Kirschner. "Cell biology. On being the right (cell) size". In: *Science (New York, N.Y.)* 348 (May 2015), p. 1245075. DOI: 10.1126/science.1245075.

[7] A. L. Hodgkin and A. F. Huxley. "A quantitative description of membrane current and its application to conduction and excitation in nerve". In: *The Journal of Physiology* 117.4 (1952), pp. 500–544. DOI: https://doi.org/10.1113/jphysiol.1952.sp004764. eprint: https://physoc.onlinelibrary.wiley.com/doi/pdf/10.1113/jphysiol.1952.sp004764. URL: https://physoc.onlinelibrary.wiley.com/doi/abs/10.1113/jphysiol.1952.sp004764.

[8] Peter Dayan and L. F. Abbott. *Theoretical Neuroscience: Computational and Mathematical Modeling of Neural Systems*. The MIT Press, 2001.

[9] A. Borisyuk and J. Rinzel. "Course 2 Understanding neuronal dynamics by geometrical dissection of minimal models". English (US). In: *Les Houches Summer School Proceedings* 80.C (2005), pp. 17–72. ISSN: 0924-8099. DOI: 10.1016/S0924-8099(05)80008-3.

[10] John Rinzel and Bard Ermentrout. "Analysis of Neural Excitability and Oscillations". In: *Methods of Neuronal Modeling* (Jan. 1998).

[11] Randall J. LeVeque. *Finite Difference Methods for Ordinary and Partial Differential Equations*. Society for Industrial and Applied Mathematics, 2007. DOI: 10.1137/1.9780898717839. eprint: https://epubs.siam.org/doi/pdf/10.1137/1.9780898717839. URL: https://epubs.siam.org/doi/abs/10.1137/1.9780898717839.

[12] The Matlab et al. "The matlab ODE suite". In: *SIAM Journal on Scientific Computing* 18 (May 1997). DOI: 10.1137/S1064827594276424.

[13] J. R. Dormand and P. J. Prince. "A family of embedded Runge-Kutta formulae". In: *Journal of Computational and Applied Mathematics* 6 (1980), pp. 19–26.

[14] James W. Cooley, F. Dodge, and H. Cohen. "Digital computer solutions for excitable membrane models". In: *Journal of Cellular and Comparative Physiology* 66 (1965), pp. 99–109.

[15] John Rinzel and Robert N. Miller. "Numerical calculation of stable and unstable periodic solutions to the Hodgkin-Huxley equations". In: *Mathematical Biosciences* 49.1 (1980), pp. 27–59. ISSN: 0025-5564. DOI: https://doi.org/10.1016/0025-5564(80)90109-1. URL: https://www.sciencedirect.com/science/article/pii/0025556480901091.